NEOPLASMA accepted, ahead of print manuscript
Cite article as https://doi.org/10.4149/neo_2026_260421N126

Running title: METTL14 promotes malignant proliferation of ES cells

METTL14 promotes the malignant proliferation of Ewing sarcoma cells and induces the M2 polarization of tumor-associated macrophages via the FOXP4-AS1/miR-107/FAM98A axis

Fangzhou He, Tingting Ren, Xiaodong Tang*

Musculoskeletal Tumor Center, Peking University People's Hospital, Beijing, China

*Correspondence: tang158776@163.com

Received April 21, 2026 / Accepted October 21, 2026

Abnormalities in the tumor immune microenvironment function as a key role in Ewing sarcoma (ES). This study aims to explain the effect of METTL14 on the polarization of tumor-associated macrophage (TAM) in the ES tumor immune microenvironment. METTL14, FOXP4-AS1, miR-107, and FAM98A were detected. Cell viability and proliferation were assayed. ES cells underwent co-culture with THP-1-induced macrophages, followed by measurement of M1 and M2 macrophage polarization, TNF-α, IL-12, IL-10, TGF-β, PCNA, iNOS, and Arg-1. FOXP4-AS1 stability was analyzed. m6A enrichment on FOXP4-AS1 was assessed. The subcellular localization of FOXP4-AS1 was detected. The bindings between FOXP4-AS1 and miR-107, as well as between miR-107 and FAM98A, were verified. METTL14, FOXP4-AS1, and FAM98A exhibited high expression, while miR-107 was lowly expressed in ES. METTL14 knockdown suppressed ES cell proliferation and promoted the M1 polarization of TAM. METTL14 promoted FOXP4-AS1 expression through m6A modification. FOXP4-AS1 bound to miR-107, and miR-107 inhibited FAM98A expression. Overexpression of FOXP4-AS1 or FAM98A, or miR-107 inhibition, could partly reverse the suppressive effect of METTL14 silencing on the ES cell proliferation and the promoting effect on the M1 polarization of TAM. In conclusion, METTL14 promotes ES cell proliferation and the M2 polarization of TAM through the FOXP4-AS1/miR-107/FAM98A axis.

Key words: Ewing sarcoma; tumor immune microenvironment; macrophage; METTL14; FOXP4-AS1

Ewing sarcoma (ES) is a highly aggressive malignant tumor of bone and soft tissue that affects children, adolescents, and young adults and is driven by the characteristic EWSR1-FLI1 chromosomal translocation [1]. Major risk factors are genetic factors and unidentified environmental contributors [2]. Despite intensive multimodal therapy comprising neoadjuvant chemotherapy, surgery or radiation, and adjuvant chemotherapy, 5-year overall survival reaches 70-80% only in localized disease and drops below 30% in metastatic or relapsed cases, underscoring the limitations of current standard-of-care approaches [3]. The tumor immune microenvironment in ES is featured by sparse T-cell infiltration and a predominance of tumor-associated macrophages (TAMs) that are polarized toward the M2 phenotype, thus enhancing tumor proliferation, angiogenesis, extracellular matrix remodeling, and immune evasion while

Accepted manuscript

suppressing anti-tumor M1 macrophage functions [4]. The M2-dominant TAM polarization within the TME sustains ES progression and contributes to therapeutic resistance [5]. Consequently, strategies that reprogram TAMs toward the anti-tumor M1 phenotype represent a promising avenue to overcome the immunosuppressive barrier in ES [6].

Methyltransferase 14 (METTL14) serves as the essential non-catalytic subunit of the N6-methyladenosine (m6A) methyltransferase complex that cooperates with METTL3 to install m6A modifications on mRNA, thereby dynamically regulating RNA splicing, stability, nuclear export, and translation efficiency [7]. METTL14 critically modulates TAM polarization within the immunosuppressive tumor immune microenvironment [8]. METTL14 activity influences the balance between anti-tumor M1 and pro-tumor M2 phenotypes through m6A-dependent control of key immune-regulatory transcripts [9]. Of note, METTL14 is significantly upregulated in tumor tissues and cell lines relative to adjacent normal tissues, with elevated levels correlating with poor patient prognosis and advanced disease stage [10]. However, the role of downstream factors mediated by METTL14-dependent m6A modification in the tumor microenvironment of ES has not been fully elucidated in current studies.

Long non-coding RNAs (lncRNAs) are transcripts that exert essential regulatory functions in gene expression, chromatin remodeling, and immune cell interactions within the tumor microenvironment [11]. LncRNA FOXP4-AS1 exerts potent tumor-promoting effects in various cancers [12-15]. LncRNA FOXP4-AS1 functions as an oncogenic regulator in ES through acting as a competing endogenous RNA (ceRNA) and modulating gene expression networks that influence cell proliferation, invasion, and immune cell interactions within the tumor microenvironment [16]. More importantly, LncRNA FOXP4-AS1 is subject to m6A modification, which dynamically regulates its stability, localization, and downstream oncogenic activity through epitranscriptomic control [17]. Given that no studies have reported lncRNA FOXP4-AS1 as a downstream factor of METTL14-mediated m6A modification in ES, we selected lncRNA FOXP4-AS1 to investigate its role in ES proliferation and the tumor microenvironment.

microRNAs (miRNAs) can post-transcriptionally regulate gene expression by binding to target mRNAs, resulting in translational repression or mRNA degradation [18]. RNA22 prediction indicated that FOXP4-AS1 has a targeted binding relationship with miR-107. miR-107 is downregulated in ES tumor tissues and cell lines compared with normal counterparts [19]. Through the ceRNA mechanism, lncRNAs competitively bind and sponge miR-107, thereby preventing miR-107 from suppressing its downstream target genes within the tumor microenvironment [20, 21]. Our preliminary screening identified family with sequence similarity 98 member A (FAM98A) as a downstream target gene of miR-107. Moreover, FAM98A is augmented in ES and enhances

Accepted manuscript

malignant proliferation of ES [22].

We investigated the role of METTL14 in ES through clinical sample collection and in vitro cell experiments. We hypothesized that METTL14 promotes the expression of FOXP4-AS1 in ES via m6A modification, thereby participating in M2 polarization of macrophages in the tumor microenvironment and malignant proliferation of ES cells through the miR-107/FAM98A axis.

Petients and methods

Ethics statement. This research gained approval from the Ethics Committee of Peking University People's Hospital (Approval No. 2018PHB170-01), and all patients signed written informed consent forms.

Collection of clinical samples. From 2020 to 2025, biopsy samples of tumor and normal tissues were collected from 22 ES patients in Peking University People's Hospital, including 10 females and 12 males, aged 10-20 years old. None of the patients had received any treatment at the time of sample collection. The samples were snap- frozen in liquid nitrogen immediately after collection and subsequently stored in a -80 °C ultra- low- temperature freezer. All samples enrolled in this study underwent molecular pathological testing during routine clinical diagnosis, and EWSR1 gene rearrangements were successfully detected in 100% of samples via FISH or RT-PCR. Detailed information is provided in Supplementary Table S1.

Cell culture. Human ES cells (A673, RD-ES, SK-ES-1), human THP-1 cells, and human mesenchymal stem cells were all purchased from ATCC (Manassas, VA, USA). A673, RD-ES, and THP-1 cells were cultured in RPMI 1640 medium (HyClone, Shanghai, China), while the other human cells were cultured in Dulbecco's modified eagle medium (DMEM, GIBCO, Waltham, MA, USA), with 1% penicillin/streptomycin and 1% gentamicin (Sigma-Aldrich, St. Louis, MO, USA). All cell lines were supplied with 10% fetal bovine serum, and underwent short tandem repeat profiling and regular test for mycoplasma contamination.

Cell treatment. Referring to a previous study [23], to mature THP-1 cells, the medium was changed to DMEM-F12 medium, with 2.5% fetal calf serum, 1% penicillin/streptomycin, and 1% gentamicin. Following standardized maturation protocol, 25 ng/ml Phorbol myristate acetate (PMA) (Sigma-Aldrich) dissolved in sterile-filtered EtOH was used to induce maturation into macrophages for 24 h, followed by a 24 h recovery period before co-culture.

In the co-culture experiment, macrophages were seeded in the lower layer of 6-well plates, while ES cells were applied to the upper layer of Transwell inserts with a 0.4 μm pore size. After 48 h of co-culture, macrophages were collected for flow cytometry, Western blot, or quantitative reverse

Accepted manuscript

transcription polymerase chain reaction (qRT-PCR) analysis, and the supernatant collected from macrophages was used for cytokine measurement.

To knockdown METTL14 expression, shRNAs targeting METTL14 and the corresponding negative controls were synthesized by HanBio Technology (Shanghai, China). The FOXP4-AS1 overexpression plasmid (oe-Lnc), FAM98A overexpression plasmid (oe-FAM98A), empty vector (oe-NC), miR-107 mimic, miR-107 inhibitor, and controls (mimic-NC, inhi-NC) were purchased from HanBio Technology. Cells were transfected with Lipofectamine® 3000 Transfection Reagent (Invitrogen, Carlsbad, CA, USA) for 48 hours before subsequent experiments.

Cell counting kit-8 (CCK-8). Cells (1×10^4) were seeded per well into 96-well plates (triplicate experiments for each group) and cultured at 37 °C and 5% CO_2. CCK-8 assay was executed at 0, 24, 48, and 72 hours. Three independent experiments were conducted for each group.

Colony formation. Cells (2×10^2) were seeded into 35 mm culture dishes and routinely cultured for 2 weeks. Cells underwent fixation with 4% paraformaldehyde solution for 20 min and staining with 0.1% crystal violet for 30 min. A cell population consisting of more than 50 cells was regarded as a colony. The number of formed colonies was counted.

qRT-PCR. Total RNA was extracted from tissues or cells via TRIzol (Invitrogen), and the analysis was performed using a Nanodrop 2000 micro ultraviolet spectrophotometer (1011U, Nanodrop). Reverse transcription primers (#4427975, Applied Biosystems, Thermo Fisher Scientific, Waltham, MA, USA) were used in the TaqMan microRNA assays. Furthermore, reverse transcription into cDNA was performed using the PrimeScript RT Kit (#RR047A, Takara, Tokyo, Japan). All primers were designed and synthesized by Takara (Table 1). Quantitative PCR detection was executed using an ABI 7500 quantitative PCR instrument (Applied biosystems) and the SYBR Green Fast PCR Kit (Applied Biosystems). The relative expression of transcripts was calculated via the $2^{-\Delta\Delta Ct}$ method [24]. For data normalization, U6 was used as the internal reference for miRNAs [25], with glyceraldehyde-3-phosphate dehydrogenase (GAPDH) as the internal reference for mRNAs and lncRNAs.

Western blot. Cells or tissues were lysed via strong radio immunoprecipitation assay buffer with protease inhibitors and phosphatase inhibitors. The lysates were centrifuged at 12,000 × g for 10 min at 4 °C to remove impurity precipitates and obtain the total protein supernatant. Same amounts of protein were isolated via sodium dodecyl sulfate polyacrylamide gel electrophoresis and transferred onto polyvinylidene fluoride membranes, subsequent to incubation with antibodies against METTL14 (1:1000, #ab309096, Abcam, Cambridge, UK), FAM98A (1:1000, #ab204083, Abcam), proliferating cell nuclear antigen (PCNA) (1:1000, #ab92552, Abcam), inducible nitric oxide synthase (iNOS) (1:1000, #ab178945, Abcam), arginase-1 (Arg-1) (1:1000, #ab133543,

Accepted manuscript

Abcam) and β-actin (1:2000, #ab8227, Abcam) at 4 °C for 12 h. Incubation with secondary antibody was conducted using immunoglobulin G (IgG) (1:2000, #ab6721, Abcam) at 25 °C for 1 h. Finally, protein bands were visualized using ECL reagent. The gray value of each band was detected and normalized to that of β-actin.

Flow cytometry. Flow cytometric staining for surface and intracellular markers was conducted following standard protocols, with data acquisition and analysis carried out on Cytoflex flow cytometer (Beckman Coulter Life Sciences, Indianapolis, Indiana, USA). Cells were incubated in Fc-block and then stained with antibodies and treated with cell stimulation cocktail (eBioscienceTM, Thermo Fisher Scientific) for 4 h prior to intracellular cytokine staining.

Prior to surface staining, cells were rinsed and stained with antibodies at 4 °C for 30 min. For intracellular staining, samples underwent fixation and permeabilization with the Cytofix/Cytoperm kit (BD Biosciences, San Jose, CA, USA) or Transcription Factor Buffer Set (BD Biosciences), and stained with intracellular antibodies at 4 °C for 30-45 min. Non-viable cells were labeled with Fixable Viability Dye 780 (BD Biosciences). IgG was used as the negative control. Flow cytometry data were assayed via the FlowJo software program. Antibodies were as follows: Alexa Fluor® 488-conjugated mouse anti-human CD68 (#ab222914, Abcam), PE/Cy7®-conjugated mouse anti-human CD206 (#ab270682, Abcam), and APC-conjugated mouse anti-human CD86 (#ab134385, Abcam).

Enzyme-linked immunosorbent assay (ELISA). After 48 h of culture, the macrophage culture medium in the lower chamber was collected, centrifuged to remove cell debris, and the resulting supernatant was harvested for ELISA analysis. The concentrations of human interleukin (IL)-10 (#MBS2568048, MyBiosource, San Diego, CA, USA), human tumor necrosis factor-alpha (TNF-α) (#MBS455676, MyBiosource), human IL-12 (#MBS2709391, MyBiosource), and human transforming growth factor beta (TGF-β) (#MBS165798, MyBiosource) were detected using ELISA kits.

Bioinformatics. The m6A modification sites on the FOXP4-AS1 sequence were analyzed online through the SRAMP database (https://www.cuilab.cn/m6asiteapp/old) [26]. The subcellular localization of FOXP4-AS1 was analyzed via the lncATLAS database (https://lncatlas.crg.eu/?tdsourcetag=s_pcqq_aiomsg) [27]. The downstream target genes of FOXP4-AS1 were predicted using the RNA22 database (https://cm.jefferson.edu/rna22/Precomputed/) [28] and LncBook 2.0 database (https://ngdc.cncb.ac.cn/lncbook/home) [29]. The downstream target genes of miR-107 were predicted by the StarBase database (https://rnasysu.com/encori/) [30], TargetScan database (https://www.targetscan.org/vert_72/) [31], miRTarBase database

Accepted manuscript

(https://awi.cuhk.edu.cn/~miRTarBase/miRTarBase_2025/php/index.php) [32] and miRWalk database (http://mirwalk.umm.uni-heidelberg.de/) [33].

RNA stability assay. Cells underwent actinomycin D (10 μg/ml) treatment for the time points (0, 4, 8, 12 h), followed by the collection of total cellular RNA. The stability of FOXP4-AS1 was determined by qRT-PCR.

Nuclear-cytoplasmic separation assay. Cytoplasmic and nuclear fractions were isolated and collected via a Nuclear/Cytoplasmic Fractionation Kit (Biovision, Milpitas, CA, USA). The RNA levels of LncRNA FOXP4-AS1, U6 (a nuclear control transcript), and GAPDH (a cytoplasmic control transcript) were assayed via qRT-PCR.

RNA binding protein immunoprecipitation (RIP). Total RNA extraction was executed by TRIzol. Next, total RNA (50 ng) was employed as the input control, and primary antibodies against IgG (#ab172730, Abcam) and m6A (#ab208577, Abcam) were applied to the remaining RNA in a buffer (150 mM NaCl, 0.1% NP-40, 10 mM Tris, RNase inhibitor). The immunoprecipitated fractions were collected using Dynabeads® Protein A (Invitrogen), rinsed with elution buffer, and retrieved via ethanol precipitation. The relative binding intensity between RNA and protein was detected via qRT-PCR and normalized against the input sample.

RNA pull down. Synthesis of biotin-labeled FOXP4-AS1 and control probes were conducted by GenePharma (Shanghai, China). Formaldehyde (1%) and glycine buffer were employed for cell cross-linking and neutralization. Total RNA underwent extraction with lysis buffer, and 50 ng of the total RNA was removed as the input control. Probes were mixed with streptavidin agarose beads (Sigma-Aldrich) using RIP buffer for 4 hours. Subsequently, cell lysates were incubated with the mixture at 4 °C overnight. Following purification, the bound RNA was validated by qRT-PCR.

Dual-luciferase reporter assay. Luciferase reporter vectors containing the wild-type and mutant FOXP4-AS1 sequences that bind to miR-107 (Lnc-WT and Lnc-MUT) were constructed, as well as the vectors containing the wild-type and mutant 3'UTR sequences of FAM98A that bind to miR-107 (FAM98A-WT and FAM98A-MUT). The above vectors were co-transfected into ES cells with miR-107 mimics or negative controls. At 48 h post-transfection, luciferase activity was detected using the dual-luciferase reporter assay system (Promega, Madison, WI, USA).

Statistical analysis. Statistical analysis and graphical visualization of all data were conducted with SPSS 21.0 (IBM SPSS Statistics, Chicago, IL, USA) and GraphPad Prism 8.0 (GraphPad Software Inc., San Diego, CA, USA). Tests for normality and homogeneity of variance were performed first, and the data conformed to a normal distribution with homogeneous variance. Data are presented as the mean±standard deviation. The chi-square test or Student's t-test was used for comparison between two groups, while one-way or two-way analysis of variance (ANOVA) was employed for

Accepted manuscript

comparison among multiple groups, with Tukey's multiple comparisons test as the post hoc test. All tests were two-sided, and $p < 0.05$ was considered statistically significant, whereas $p < 0.01$ was considered highly statistically significant.

Results

METTL14 knockdown suppresses the malignant proliferation of ES cells. We detected METTL14 expression in ES tissues and found that METTL14 was highly expressed in ES tumor tissues compared with adjacent normal tissues ($p < 0.01$, Figures 1A, 1B). METTL14 also showed a high expression in multiple ES cell lines ($p < 0.01$, Figures 1C, 1D). We reduced METTL14 expression in A673 and RD-ES cells ($p < 0.01$, Figures 1E, 1F), and subsequently observed lowered cell viability ($p < 0.01$, Figure 1G), reduced colony formation capacity ($p < 0.01$, Figure 1H), and downregulated PCNA expression ($p < 0.01$, Figure 1I). Collectively, knockdown of METTL14 suppresses the malignant proliferation of ES cells.

Knockdown of METTL14 in ES cells promotes M1 polarization of TAMs. We co-cultured differentially transfected A673 cells and RD-ES cells with macrophages derived from PMA-induced THP-1 cells, respectively. After co-culture, flow cytometry detection of macrophages harvested from the lower chamber showed that METTL14 knockdown promoted M1 macrophage polarization in A673 cells and RD-ES cells, with an increased proportion of $CD86^+$ cells and a decreased proportion of $CD206^+$ cells ($p < 0.05$, Figure 2A). ELISA detection of culture supernatants harvested from macrophages in the lower chamber revealed elevated levels of TNF-α and IL-12 in macrophage-conditioned medium ($p < 0.01$, Figure 2B) and reduced IL-10 and TGF-β levels ($p < 0.01$, Figure 2B). Meanwhile, the intracellular level of the M1 marker enzyme iNOS was upregulated, while the expression of the M2-related enzyme Arg-1 was downregulated in macrophages ($p < 0.01$, Figure 2C). Furthermore, the culture medium of METTL14-silenced A673 cells was replaced with the macrophage-conditioned medium after the co-culture. The results demonstrated that the conditioned medium from M1-polarized macrophages (sh-METTL14-CM) further inhibited the proliferation of A673 cells ($p < 0.05$, Figures 2D-2F). Collectively, ES cells with METTL14 knockdown shows suppressed cell proliferation, which may contribute to its function of promoting M1 polarization of TAMs in the tumor microenvironment.

METTL14 promotes lncRNA FOXP4-AS1 expression via m6A modification. Bioinformatics prediction using the SRAMP database revealed m6A modification sites on lncRNA FOXP4-AS1 (Figure 3A). FOXP4-AS1 exhibited high expression in ES tissues and cell lines ($p < 0.01$, Figures 3B, 3C). Further investigations demonstrated that METTL14 knockdown significantly reduced m6A enrichment on FOXP4-AS1 ($p < 0.01$, Figure 3D), lowered FOXP4-AS1 stability ($p < 0.01$,

Accepted manuscript

Figure 3E), and downregulated FOXP4-AS1 expression ($p < 0.01$, Figure 3F). Collectively, METTL14 promotes FOXP4-AS1 expression in ES cells via m6A modification.

FOXP4-AS1 overexpression partially reverses the inhibitory effect of METTL14 knockdown on ES progression. Subsequently, we upregulated FOXP4-AS1 in A673 cells ($p < 0.01$, Figures 4A, 4B) and conducted rescue experiments with METTL14 knockdown to verify the above mechanism. Compared with METTL14 knockdown alone, FOXP4-AS1 overexpression increased cell viability ($p < 0.01$, Figure 4C), enhanced colony formation capacity ($p < 0.01$, Figure 4D), and upregulated PCNA expression ($p < 0.01$, Figure 4E). After co- culturing macrophages with A673 cells subjected to METTL14 knockdown combined with FOXP4- AS1 overexpression, the proportion of $CD86^+$ cells decreased and the proportion of $CD206^+$ cells increased in macrophages in the lower chamber, compared with A673 cells with METTL14 knockdown alone ($p < 0.01$, Figure 4F). TNF-α and IL-12 were lowered in the supernatants of macrophages located in the lower chamber ($p < 0.01$, Figure 4G), while IL-10 and TGF-β were increased ($p < 0.05$, Figure 4G). Intracellular iNOS expression was reduced, while Arg-1 expression was elevated in macrophages ($p < 0.01$, Figure 4H). Taken together, after METTL14 knockdown, FOXP4-AS1 overexpression partially counteracts the suppressive effect of METTL14 knockdown on ES cell proliferation and the promoting effect on M1 polarization of TAMs.

LncRNA FOXP4-AS1 binds to miR-107, and miR-107 inhibits FAM98A expression. Database prediction indicated that the subcellular localization of FOXP4-AS1 was in the cytoplasm (Figure 5A). Nuclear-cytoplasmic separation assays verified that FOXP4-AS1 was abundantly expressed within the cytoplasm ($p < 0.01$, Figure 5B), suggesting that FOXP4-AS1 exerts its cellular functions via the ceRNA mechanism. Venn diagram analysis showed 133 targeted miRNAs downstream of FOXP4-AS1 after screening by two databases (Figure 5A). Literature review revealed that miR-107 was lowly expressed in ES [19]. miR-107 was downregulated in ES tissues and cells ($p < 0.01$, Figures 6A, 6B) and was negatively related with FOXP4-AS1 expression ($p < 0.01$, Figure 6E). FOXP4-AS1 could bind to miR-107 ($p < 0.01$, Figure 5C). Dual-luciferase reporter assays verified the interaction between FOXP4-AS1 and miR-107 and the binding between miR-107 and the 3'UTR sequence of FAM98A ($p < 0.01$, Figure 5D). Knockdown of METTL14 increased intracellular miR-107 expression ($p < 0.01$, Figures 6C, 6D), while overexpression of FOXP4-AS1 suppressed miR-107 expression ($p < 0.01$, Figure 6C).

Subsequently, Venn diagram analysis revealed that 84 downstream target genes of miR-107 were overlapped within the intersection (Figure 5A). Literature research indicated that FAM98A was highly expressed in ES [22]. Detection in ES tissues and cell lines confirmed the upregulation of FAM98A in ES ($p < 0.01$, Figures 6A, 6B, 6F, 6G). FAM98A expression was positively related with

Accepted manuscript

FOXP4-AS1 expression ($p < 0.01$, Figure 6E) and negatively associated with miR-107 expression ($p < 0.05$, Figure 6E). METTL14 knockdown significantly decreased FAM98A expression, while FOXP4-AS1 overexpression increased FAM98A expression ($p < 0.01$, Figures 6C, 6D, 6H, 6I). FOXP4-AS1 targets and binds to miR-107, and miR-107 targets and inhibits FAM98A expression in ES cells.

miR-107 inhibition partially reverses the suppressive effect of METTL14 knockdown on ES progression. We transfected cells with miR-107 inhibitor to downregulate miR-107 expression in A673 cells ($p < 0.01$, Figures 7A, 7B) and performed combined treatment with METTL14 knockdown. Compared with METTL14 knockdown alone, combined treatment significantly upregulated intracellular FAM98A expression ($p < 0.01$, Figures 7B, 7C), enhanced cell viability ($P < 0.01$, Figure 7D), promoted colony formation capacity ($p < 0.01$, Figure 7E), and promoted PCNA expression ($P < 0.01$, Figure 7C). After co-culture of A673 cells with decreased METTL14 expression and miR-107 inhibition with macrophages, the proportion of $CD86^+$ macrophages was decreased while the proportion of $CD206^+$ macrophages was increased in macrophages from the lower chamber ($p < 0.05$, Figure 7F). TNF-α and IL-12 were reduced in the supernatants of macrophages from the lower chamber ($p < 0.01$, Figure 7G), whereas IL-10 and TGF-β were increased ($p < 0.05$, Figure 7G). Intracellular iNOS expression was decreased, while Arg-1 expression was increased in macrophages ($P < 0.01$, Figure 7H). These results suggest that after METTL14 knockdown, inhibition of miR-107 partially counteracts the suppressive effect of METTL14 knockdown on ES cell proliferation and the promoting effect on M1 polarization of TAMs.

FAM98A overexpression partially reverses the inhibitory effect of METTL14 knockdown on ES progression. Finally, we conducted FAM98A overexpression in A673 cells ($p < 0.01$, Figures 8A-8C) and performed combined treatment with METTL14 knockdown. Compared with sole METTL14 knockdown, the combined treatment group demonstrated enhanced cell viability ($p < 0.01$, Figure 8D), increased colony formation capacity ($p < 0.01$, Figure 8E), and upregulated PCNA expression ($p < 0.01$, Figure 8C). After co-culture of A673 cells with decreased METTL14 expression and overexpression of FAM98A with macrophages, $CD86^+$ macrophage proportion was reduced while the proportion of $CD206^+$ macrophages was increased in macrophages within the lower chamber ($p < 0.01$, Figure 8F). TNF-α and IL-12 were reduced in the supernatants of macrophages located in the lower chamber ($p < 0.01$, Figure 8G), whereas IL-10 and TGF-β were increased ($p < 0.05$, Figure 8G). Intracellular iNOS expression was downregulated, whereas Arg-1 expression was upregulated in macrophages ($p < 0.01$, Figure 8H). Taken together, after METTL14 knockdown, FAM98A overexpression partially counteracts the suppressive effect of METTL14

Accepted manuscript

knockdown on malignant proliferation of ES cells and the promoting effect on M1 polarization of TAMs.

Discussion

TAMs are critical regulators within the tumor microenvironment and undergo polarization into two functionally opposing phenotypes [4]. Classically activated M1 macrophages are characterized by the surface marker CD86 and secretion of pro-inflammatory cytokines such as TNF-α, IL-12, and iNOS that exert direct anti-tumor cytotoxicity and activate adaptive immune responses [34]. Activated M2 macrophages are marked by CD206 and produce immunosuppressive factors including IL-10, TGF-β, and Arg-1 that promote tumor cell proliferation, angiogenesis, extracellular matrix remodeling, and immune evasion [35, 36]. In ES, the tumor immune microenvironment is dominated by M2-polarized TAMs, which sustain malignant proliferation and therapeutic resistance while limiting anti-tumor M1 functions [6]. Consequently, an increased proportion of $CD86^+$ M1 TAMs coupled with a decreased proportion of $CD206^+$ M2 TAMs signifies a beneficial phenotypic switch that enhances anti-tumor immunity and inhibits ES cell growth. Here, METTL14 knockdown suppresses malignant proliferation of ES cells and reprograms TAMs toward M1 polarization via the FOXP4-AS1/miR-107/FAM98A axis.

METTL14 functions as a pro-oncogenic m6A writer that drives tumor proliferation and sustains an immunosuppressive tumor microenvironment in ES [10]. Additionally, in cervical cancer, elevated METTL14 promotes PD-1^+ M2-like TAM accumulation, impairing macrophage phagocytosis and facilitating immune evasion [37]. METTL14 promotes the malignant proliferation of DTX-resistant lung cancer cells and M2 polarization by enhancing m6A methylation of DKK4 mRNA, thereby strengthening resistance to DTX [38]. METTL14 knockout enhances the activation and infiltration of $CD8^+$ T cells in the lung cancer, augments the response to PD-1 immunotherapy, and suppresses lung cancer progression [39]. Here, METTL14 is highly expressed in ES samples. METTL14 knockdown suppresses ES cell malignant proliferation while reprogramming TAMs toward the anti-tumor M1 phenotype, with increased $CD86^+$ proportion, M1 cytokines, decreased $CD206^+$ proportion, and M2 cytokines.

METTL14 promotes lncRNA FOXP4-AS1 expression via m6A modification in ES cells, as evidenced by reduced m6A enrichment, decreased transcript stability, and downregulated FOXP4-AS1 levels upon METTL14 knockdown. FOXP4-AS1 overexpression partly counteracts the suppressive effects of METTL14 knockdown on ES cell malignant proliferation and M1 TAM polarization, restoring cell viability, colony formation, PCNA expression, $CD206^+$ M2 proportions, and immunosuppressive cytokine profiles. A previous study has confirmed that in the tumor

Accepted manuscript

353 microenvironment of ES, FOXP4-AS1 modulates immune infiltrates by favoring
354 immunosuppressive M2 TAM polarization and potentially acting through extracellular
355 vesicle-mediated mechanisms to promote immune evasion and tumor progression [16]. LncRNA
356 FOXP4-AS1 exerts oncogenic functions in multiple cancers [40]. Low expression of FOXP4-AS1 is
357 related to favorable therapeutic outcomes in patients with hepatocellular carcinoma and can
358 suppress the invasion, migration and angiogenesis of cancer cells [12]. Upregulated FOXP4-AS1
359 inhibits the viability of tumor-infiltrating $CD8^+$ T cells in esophageal carcinoma, suppresses their
360 cytotoxicity and promotes T cell exhaustion, thereby leading to immune escape and tumor growth
361 [41]. In prostate cancer, patients with high FOXP4-AS1 expression present poor prognosis and
362 FOXP4-AS1 serves as a ceRNA to sponge miR-3184-5p and upregulates FOXP4, promoting
363 proliferation and restraining apoptosis of prostate cancer cells [14]. Consistently, the present study
364 positions METTL14-dependent m6A stabilization of FOXP4-AS1 as a critical upstream regulator
365 that links epitranscriptomic control to ceRNA-mediated immune reprogramming in the ES tumor
366 microenvironment.
367 Subsequently, we confirmed that FOXP4-AS1 binds to and inhibits miR-107 in ES cells. The
368 miR-107 inhibitor promotes M2 polarization of TAMs and rescues the malignant proliferation of ES
369 cells. miR-107 functions as a tumor suppressor in ES and multiple malignancies. In ES, miR-107 is
370 significantly downregulated and targets HIF-1β to inhibit cell proliferation, tube formation,
371 cell-cycle progression, and promote apoptosis [19]. In colorectal cancer, miR-107 is downregulated
372 and suppresses metastasis by inhibiting TFR1, positioning it as a potential therapeutic target [42].
373 Intratumoral injection of miR-107 prodrug in gastric cancer can target CGA and GATA2, suppress
374 the downstream signaling transduction of epidermal growth factor receptor, and enhance the
375 sensitivity to chemotherapeutic drugs [43]. In hypopharyngeal squamous cell carcinoma, miR-107
376 targets and inhibits NSG1, thereby downregulating the ERK signaling, inhibiting cell proliferation,
377 migration and invasion, and enhancing apoptosis [44]. A previous in vivo study has demonstrated
378 that the c-Myc inhibitor JQ1 suppresses tumor cell migration induced by M2 macrophage-derived
379 exosomes by interfering with miR-107 [45]. Importantly, accumulating evidence indicates that
380 lncRNAs upregulate downstream oncogenic factors by sponging miR-107 via the ceRNA
381 mechanism, activate M2 polarization in cancer, and promote the proliferation and invasion of
382 cancer cells [46, 47]. In this study, miR-107 targets and inhibits the expression of FAM98A.
383 FAM98A has been widely validated as an oncogene that inhibits ferroptosis in cancer cells,
384 enhances cell proliferation, promotes tumorigenesis, and contributes to chemoresistance [48, 49].
385 LncRNA FOXP4-AS1 may sponge miR-107 through the ceRNA mechanism, thereby restoring
386 FAM98A expression, promoting M2 polarization of TAMs, and accelerating the malignant

Accepted manuscript

proliferation of ES cells.

We need to elaborate on several limitations of the present study. Due to resource constraints, we only selected miR-107 as the downstream target of FOXP4-AS1 and FAM98A as the downstream target of miR-107 for investigation, and comprehensive mechanistic and functional validation of other potential target genes has not been carried out. In vivo data would undoubtedly provide more convincing evidence to corroborate this polarization phenotype. Nevertheless, limited by time and experimental conditions, we failed to conduct in vivo studies in the present work. As cell-level experiments cannot fully mimic the tumor immune microenvironment in vivo, the conclusions of our study cannot be directly used for clinical translation. Meanwhile, the small sample size of clinical specimens restricts the clinical translation of our findings. Meanwhile, we will establish in vivo xenograft tumor models. Immunohistochemistry will be used to detect polarization markers (F4/80, CD86, CD206) of tumor-infiltrating macrophages, so as to confirm this phenotype within the in vivo microenvironment. Although we only collected conditioned medium from lower-chamber macrophages for ELISA measurement, and the Transwell membrane prohibited physical mixing of two cell populations, we acknowledge that soluble cytokines can theoretically diffuse across the membrane. Therefore, trace cytokine contributions derived from upper-chamber tumor cells cannot be completely excluded at the protein level. In future investigations, intracellular cytokine staining combined with flow cytometry will be adopted to precisely trace the cellular origin of these cytokines. Moreover, we will enlarge the clinical sample size in future studies to enhance the universality of our findings. In addition, we will further explore more downstream target genes of METTL14, FOXP4-AS1, and miR-107.

In conclusion, METTL14 is highly expressed in ES. Knockdown of METTL14 suppresses the malignant proliferation of ES cells and promotes M1 polarization of TAMs through the FOXP4-AS1/miR-107/FAM98A axis.

Acknowledgements: This work was supported by Peking University People's Hospital Scientific Research Development Funds (RDJP2025-18) and Noncommunicable Chronic Diseases-National Science and Technology Major Project (No.2024ZD0525801).

Supplementary data are available in the online version of the paper.

References

[1] GRUNEWALD TGP, CIDRE-ARANAZ F, SURDEZ D, TOMAZOU EM, DE ALAVA E et al. Ewing sarcoma. Nat Rev Dis Primers 2018; 4: 5. https://doi.org/10.1038/s41572-018-0003-x

Accepted manuscript

[2] GARGALLO P, YANEZ Y, JUAN A, SEGURA V, BALAGUER J et al. Review: Ewing Sarcoma Predisposition. Pathol Oncol Res 2020; 26: 2057-2066. https://doi.org/10.1007/s12253-019-00765-3
[3] HESLA AC, PAPAKONSTANTINOU A, TSAGKOZIS P. Current Status of Management and Outcome for Patients with Ewing Sarcoma. Cancers (Basel) 2021; 13: 1202. https://doi.org/10.3390/cancers13061202
[4] EVDOKIMOVA V, GASSMANN H, RADVANYI L, BURDACH SEG. Current State of Immunotherapy and Mechanisms of Immune Evasion in Ewing Sarcoma and Osteosarcoma. Cancers (Basel) 2022; 15: 272. https://doi.org/10.3390/cancers15010272
[5] MORALES E, OLSON M, IGLESIAS F, DAHIYA S, LUETKENS T et al. Role of immunotherapy in Ewing sarcoma. J Immunother Cancer 2020; 8: e000653. https://doi.org/10.1136/jitc-2020-000653
[6] KUMAR RR, AGARWAL N, SHREE A, GORAIN JK, RAHUL E et al. Decoding the immune landscape in Ewing sarcoma pathogenesis: The role of tumor infiltrating immune cells and immune milieu. J Bone Oncol 2025; 52: 100678. https://doi.org/10.1016/j.jbo.2025.100678
[7] ZHANG L, HOU C, CHEN C, GUO Y, YUAN W et al. The role of N(6)-methyladenosine (m(6)A) modification in the regulation of circRNAs. Mol Cancer 2020; 19: 105. https://doi.org/10.1186/s12943-020-01224-3
[8] DONG L, CHEN C, ZHANG Y, GUO P, WANG Z et al. The loss of RNA N(6)-adenosine methyltransferase Mettl14 in tumor-associated macrophages promotes CD8(+) T cell dysfunction and tumor growth. Cancer Cell 2021; 39: 945-957e910. https://doi.org/10.1016/j.ccell.2021.04.016
[9] WANG M, XIE Z, TAN Y, ZHOU Y, WANG S et al. METTL14 knockdown augmented the polarization of M2-like macrophages to promote acute myeloid leukemia progression. Hum Cell 2025; 38: 168. https://doi.org/10.1007/s13577-025-01300-0
[10] JIANG J, FAN Q, QU H, LIU C, LIANG T et al. Novel prognostic biomarkers, METTL14 and YTHDF2, associated with RNA methylation in Ewing's sarcoma. Sci Rep 2022; 12: 7041. https://doi.org/10.1038/s41598-022-06744-0
[11] XU Z, CHEN Y, MA L, CHEN Y, LIU J et al. Role of exosomal non-coding RNAs from tumor cells and tumor-associated macrophages in the tumor microenvironment. Mol Ther 2022; 30: 3133-3154. https://doi.org/10.1016/j.ymthe.2022.01.046
[12] LIANG J, WANG D, QIU G, ZHU X, LIU J et al. Long Noncoding RNA FOXP4-AS1 Predicts Unfavourable Prognosis and Regulates Proliferation and Invasion in Hepatocellular Carcinoma. Biomed Res Int 2021; 2021: 8850656. https://doi.org/10.1155/2021/8850656
[13] TAO HF, SHEN JX, HOU ZW, CHEN SY, SU YZ et al. lncRNA FOXP4- AS1 predicts poor prognosis and accelerates the progression of mantle cell lymphoma through the miR- 423- 5p/NACC1 pathway. Oncol Rep 2021; 45: 469-480. https://doi.org/10.3892/or.2020.7897
[14] WU X, XIAO Y, ZHOU Y, ZHOU Z, YAN W. LncRNA FOXP4-AS1 is activated by PAX5 and promotes the growth of prostate cancer by sequestering miR-3184-5p to upregulate FOXP4. Cell Death Dis 2019; 10: 472. https://doi.org/10.1038/s41419-019-1699-6
[15] ZHAO J, YANG T, LI L. LncRNA FOXP4-AS1 Is Involved in Cervical Cancer Progression via Regulating miR-136-5p/CBX4 Axis. Onco Targets Ther 2020; 13: 2347-2355.

Accepted manuscript

https://doi.org/10.2147/OTT.S241818
[16] XIONG J, WU L, HUANG L, WU C, LIU Z et al. LncRNA FOXP4-AS1 Promotes Progression of Ewing Sarcoma and Is Associated With Immune Infiltrates. Front Oncol 2021; 11: 718876. https://doi.org/10.3389/fonc.2021.718876
[17] CUSENZA VY, TAMENI A, NERI A, FRAZZI R. The lncRNA epigenetics: The significance of m6A and m5C lncRNA modifications in cancer. Front Oncol 2023; 13: 1063636. https://doi.org/10.3389/fonc.2023.1063636
[18] HILL M, TRAN N. miRNA interplay: mechanisms and consequences in cancer. Dis Model Mech 2021; 14: dmm047662. https://doi.org/10.1242/dmm.047662
[19] CHEN J, ZHOU X, XIAO Q, WANG T, SHAO G et al. MiR-107 suppresses cell proliferation and tube formation of Ewing sarcoma cells partly by targeting HIF-1beta. Hum Cell 2018; 31: 42-49. https://doi.org/10.1007/s13577-017-0183-9
[20] FANG J, LI K, HUANG C, XUE H, NI Q. LncRNA TTN-AS1 confers tamoxifen resistance in breast cancer via sponging miR-107 to modulate PI3K/AKT signaling pathway. Am J Transl Res 2022; 14: 2267-2279.
[21] ZHANG Q, CHEN Z. lncRNA UASR1 sponges miR-107 in colorectal cancer to upregulate oncogenic CDK8 and promote cell proliferation. Oncol Lett 2020; 20: 305. https://doi.org/10.3892/ol.2020.12168
[22] JI Y, GAO T, XU Z, CHEN B, LI K. Kaempferol regulates Ewing sarcoma progression via miR-26b-5p-mediated expression of the family with sequence similarity 98 member A. BMC Pharmacol Toxicol 2025; 26: 167. https://doi.org/10.1186/s40360-025-01008-9
[23] RAUCHENWALD T, HANDLE F, CONNOLLY CE, DEGEN A, SEIFARTH C et al. Preadipocytes in human granulation tissue: role in wound healing and response to macrophage polarization. Inflamm Regen 2023; 43: 53. https://doi.org/10.1186/s41232-023-00302-5
[24] LIVAK KJ, SCHMITTGEN TD. Analysis of relative gene expression data using real-time quantitative PCR and the 2(-Delta Delta C(T)) Method. Methods 2001; 25: 402-408. https://doi.org/10.1006/meth.2001.1262
[25] WANG XJ, ZHANG D, YANG YT, LI XY, LI HN et al. Suppression of microRNA-222-3p ameliorates ulcerative colitis and colitis-associated colorectal cancer to protect against oxidative stress via targeting BRG1 to activate Nrf2/HO-1 signaling pathway. Front Immunol 2023; 14: 1089809. https://doi.org/10.3389/fimmu.2023.1089809
[26] FAN R, CUI C, KANG B, CHANG Z, WANG G et al. A combined deep learning framework for mammalian m6A site prediction. Cell Genom 2024; 4: 100697. https://doi.org/10.1016/j.xgen.2024.100697
[27] MAS-PONTE D, CARLEVARO-FITA J, PALUMBO E, HERMOSO PULIDO T, GUIGO R et al. LncATLAS database for subcellular localization of long noncoding RNAs. RNA 2017; 23: 1080-1087. https://doi:10.1261/rna.060814.117
[28] MIRANDA KC, HUYNH T, TAY Y, ANG YS, TAM WL et al. A pattern-based method for the identification of MicroRNA binding sites and their corresponding heteroduplexes. Cell 2006; 126: 1203-1217. https://doi.org/10.1016/j.cell.2006.07.031
[29] LI Z, LIU L, FENG C, QIN Y, XIAO J et al. LncBook 2.0: integrating human long non-coding RNAs with multi-omics annotations. Nucleic Acids Res 2023; 51: D186-D191. https://doi.org/10.1093/nar/gkac999

Accepted manuscript

[30] LI JH, LIU S, ZHOU H, QU LH, YANG JH. starBase v2.0: decoding miRNA-ceRNA, miRNA-ncRNA and protein-RNA interaction networks from large-scale CLIP-Seq data. Nucleic Acids Res 2014; 42: D92-97. https://doi.org/10.1093/nar/gkt1248

[31] AGARWAL V, BELL GW, NAM JW, BARTEL DP. Predicting effective microRNA target sites in mammalian mRNAs. Elife 2015; 4: e05005. https://doi.org/10.7554/eLife.05005

[32] CUI S, YU S, HUANG HY, LIN YC, HUANG Y et al. miRTarBase 2025: updates to the collection of experimentally validated microRNA-target interactions. Nucleic Acids Res 2025; 53: D147-D156. https://doi.org/10.1093/nar/gkae1072

[33] STICHT C, DE LA TORRE C, PARVEEN A, GRETZ N. miRWalk: An online resource for prediction of microRNA binding sites. PLoS One 2018; 13: e0206239. https://doi.org/10.1371/journal.pone.0206239

[34] KANG JH, KIM JH, GIM JA, LEE MY. iNOS in Macrophage Polarization: Pharmacological and Regulatory Insights. Int J Mol Sci 2025; 26: 12056. https://doi.org/10.3390/ijms262412056

[35] MARTINENAITE E, LECOQ I, AABOE-JORGENSEN M, AHMAD SM, PEREZ-PENCO M et al. Arginase-1-specific T cells target and modulate tumor-associated macrophages. J Immunother Cancer 2025; 13:e009930. https://doi.org/10.1136/jitc-2024-009930

[36] WEIL R, LOEB D. Breaking down the tumor immune infiltration within pediatric sarcomas. Front Endocrinol (Lausanne) 2023; 14: 1187289. https://doi.org/10.3389/fendo.2023.1187289

[37] WANG B, MAO Z, YE J, JIAO X, ZHANG T et al. Glycolysis Induced by METTL14 Is Essential for Macrophage Phagocytosis and Phenotype in Cervical Cancer. J Immunol 2024; 212: 723-736. https://doi.org/10.4049/jimmunol.2300339

[38] YANG X, SONG Y, SUN Q, HAN F, ZHUANG X. METTL14 Mediates Malignant Progression and Docetaxel Resistance of Lung Cancer by Regulating DKK4 Expression Through m6A Methylation Modification. J Biochem Mol Toxicol 2025; 39: e70587. https://doi.org/10.1002/jbt.70587

[39] SUN C, WANG J, LI H, LIU L, LIN Y et al. METTL14 regulates CD8(+)T-cell activation and immune responses to anti-PD-1 therapy in lung cancer. World J Surg Oncol 2024; 22: 128. https://doi.org/10.1186/s12957-024-03402-9

[40] YANG J. Emerging roles of long non-coding RNA FOXP4-AS1 in human cancers: From molecular biology to clinical application. Heliyon 2024; 10: e39857. https://doi.org/10.1016/j.heliyon.2024.e39857

[41] SHEN GY, ZHANG Y, HUANG RZ, HUANG ZY, YANG LY et al. FOXP4-AS1 promotes CD8(+) T cell exhaustion and esophageal cancer immune escape through USP10-stabilized PD-L1. Immunol Res 2024; 72: 766-775. https://doi.org/10.1007/s12026-024-09482-9

[42] FU Y, LIN L, XIA L. MiR-107 function as a tumor suppressor gene in colorectal cancer by targeting transferrin receptor 1. Cell Mol Biol Lett 2019; 24: 31. https://doi.org/10.1186/s11658-019-0155-z

[43] WANG P, ZHOU Y, WANG J, ZHOU Y, ZHANG X et al. miR-107 reverses the multidrug resistance of gastric cancer by targeting the CGA/EGFR/GATA2 positive feedback circuit. J Biol Chem 2024; 300: 107522. https://doi.org/10.1016/j.jbc.2024.107522

[44] HU Y, HE Z, HAN B, LIN Z, ZHOU P et al. miR-107 Targets NSG1 to Regulate Hypopharyngeal Squamous Cell Carcinoma Progression through ERK Pathway. Int J Mol Sci

Accepted manuscript

2024; 25: 5961. https://doi.org/10.3390/ijms25115961
[45] ZHOU X, LIU X, YANG X, WANG L, HONG Y et al. Tumor progress intercept by intervening in Caveolin-1 related intercellular communication via ROS-sensitive c-Myc targeting therapy. Biomaterials 2021; 275: 120958. https://doi.org/10.1016/j.biomaterials.2021.120958
[46] LIU P, GAO X, YU Z, LIU Y, LIU Y et al. H19 promotes polarization and alternative splicing in tumor-associated macrophages, facilitating pancreatic cancer progression. Cancer Lett 2024; 611: 217389. https://doi.org/10.1016/j.canlet.2024.217389
[47] TIAN X, WU Y, YANG Y, WANG J, NIU M et al. Long noncoding RNA LINC00662 promotes M2 macrophage polarization and hepatocellular carcinoma progression via activating Wnt/beta-catenin signaling. Mol Oncol 2020; 14: 462-483. https://doi.org/10.1002/1878-0261.12606
[48] LI Z, LI N, SUN X, WANG J. FAM98A promotes cancer progression in endometrial carcinoma. Mol Cell Biochem 2019; 459: 131-139. https://doi.org/10.1007/s11010-019-03556-1
[49] HE Z, YANG J, SUI C, ZHANG P, WANG T et al. FAM98A promotes resistance to 5-fluorouracil in colorectal cancer by suppressing ferroptosis. Arch Biochem Biophys 2022; 722: 109216. https://doi.org/10.1016/j.abb.2022.109216

Figure Legends

Figure 1. METTL14 knockdown suppresses the malignant proliferation of ES cells. A, B) The expression of METTL14 in tumor tissues from ES patients was detected by qRT-PCR and Western blot, with paired adjacent normal tissues as controls, n=22; C, D) The expression of METTL14 in hMSCs and ES cell lines A673, RD-ES, and SK-ES-1 was detected by qRT-PCR and Western blot, n=3; shRNA targeting METTL14 (sh-METTL14) was transfected into A673 and RD-ES cells, with sh-NC as the control; E, F)The expression of METTL14 was detected by qRT-PCR and Western blot, n=3; G: Cell viability was determined by CCK-8 assay, n=3; H) Cell proliferation was evaluated by colony formation assay, n=3; I) The expression of PCNA was detected by Western blot, n=3; Data are presented as the mean±standard deviation. Student's t-test was used for panels A-B, one-way ANOVA was used for panels C-D, and two-way ANOVA was used for panels E-I, with Tukey's multiple comparisons test as the post hoc test. $^{**}p < 0.01$

Figure 2. Knockdown of METTL14 in ES cells promotes M1 polarization of TAMs. THP-1 cells were induced into macrophages by PMA and then co-cultured with differentially transfected A673 cells and RD-ES cells. A) The proportions of $CD86^{+}CD68^{+}$ and $CD206^{+}CD68^{+}$ cells were detected by flow cytometry; B) Transwell lower-chamber macrophage supernatants were harvested and centrifuged; the levels of TNF-α, IL-12, IL-10, and TGF-β in the supernatant were measured by ELISA; C) The expression of iNOS and Arg-1 was detected by Western blot; The culture medium of

Accepted manuscript

A673 cells transfected with sh-METTL14 was replaced with the conditioned medium after co-culture (sh-NC-CM, sh-METTL14-CM). D) Cell viability was determined by CCK-8 assay; E) Cell proliferation was evaluated by colony formation assay; F) The expression of PCNA was detected by Western blot; n=3. Data are presented as the mean±standard deviation. Student's t-test was used for panel B, one-way ANOVA was used for panels E-F, and two-way ANOVA was used for panels A, C, and D, with Tukey's multiple comparisons test as the post hoc test. *$p < 0.05$, **$p < 0.01$

Figure 3. METTL14 promotes lncRNA FOXP4-AS1 expression through m6A modification. A) The m6A modification sites in the FOXP4-AS1 sequence were analyzed online using the SRAMP database; B) The expression of FOXP4-AS1 in tumor tissues from ES patients was detected by qRT-PCR, with paired adjacent normal tissues as controls, n=22; C) The expression of FOXP4-AS1 in hMSCs and ES cell lines A673, RD-ES, and SK-ES-1 was detected by qRT-PCR, n=3; D) The enrichment of m6A on FOXP4-AS1 was detected by RIP assay, n=3; E) The stability of FOXP4-AS1 was examined after actinomycin D treatment, n=3; F) The expression of FOXP4-AS1 in cells with different treatments was detected by qRT-PCR, n=3; Data are presented as the mean±standard deviation. Student's t-test was used for panel B, one-way ANOVA was used for panel C, and two-way ANOVA was used for panels D-F, with Tukey's multiple comparisons test as the post hoc test. **$p < 0.01$

Figure 4. FOXP4-AS1 overexpression partially reverses the inhibitory effect of METTL14 knockdown on ES progression. A673 cells were transfected with FOXP4-AS1 overexpression vector (oe-Lnc) using empty vector (oe-NC) as control, followed by combined treatment with sh-METTL14. A, B) The expression of FOXP4-AS1 was detected by qRT-PCR; C) Cell viability was determined by CCK-8 assay; D) Cell proliferation was evaluated by colony formation assay; E) The expression of PCNA was detected by Western blot; Subsequently, cells were co-cultured with macrophages. F) The proportions of $CD86^+CD68^+$ and $CD206^+CD68^+$ cells were detected by flow cytometry; G: Transwell lower-chamber macrophage supernatants were harvested and centrifuged; the levels of TNF-α, IL-12, IL-10 and TGF-β in the supernatant were measured by ELISA; H: The expression of iNOS and Arg-1 was detected by Western blot; n=3. Data are presented as the mean±standard deviation. Student's t-test was used for panel A, one-way ANOVA was used for panels B, D, E and G, and two-way ANOVA was used for panels C, F and H, with Tukey's multiple comparisons test as the post hoc test. *$p < 0.05$, **$p < 0.01$.

Figure 5. LncRNA FOXP4-AS1 binds to miR-107, and miR-107 inhibits FAM98A expression. A)

Accepted manuscript

The subcellular localization of FOXP4-AS1 was analyzed using the lncATLAS database. The downstream target genes of FOXP4-AS1 were predicted by the RNA22 and LncBook 2.0 databases, and the downstream target genes of miR-107 were predicted by the StarBase, TargetScan, miRTarBase and miRWalk databases; B) The subcellular localization of FOXP4-AS1 was detected by nuclear-cytoplasmic separation assay, n=3; C) The binding between FOXP4-AS1 and miR-107 was examined by RNA pull-down assay, n=3; D) The binding relationships between FOXP4-AS1 and miR-107, as well as between miR-107 and the 3'UTR sequence of FAM98A, were detected by dual-luciferase reporter assay, n=3; Student's t-test was used for panel C, and two-way ANOVA was used for panel D, with Tukey's multiple comparisons test as the post hoc test. $^{**}p < 0.01$

Figure 6. LncRNA FOXP4-AS1 binds to miR-107, and miR-107 inhibits FAM98A expression. A) The expression of miR-107 and FAM98A in tumor tissues from ES patients was detected by qRT-PCR, with paired adjacent normal tissues as controls, n=22; B) The expression of miR-107 and FAM98A in hMSCs and ES cell lines A673, RD-ES and SK-ES-1 was detected by qRT-PCR, n=3; C, D) The expression of miR-107 and FAM98A in cells with different treatments was detected by qRT-PCR, n=3; E) Pearson correlation analysis was performed for the expression of FOXP4-AS1, miR-107 and FAM98A in tumor tissues from ES patients; F) The expression of FAM98A in tumor tissues from ES patients was detected by Western blot, n=22; G) The expression of FAM98A in hMSCs and ES cell lines A673, RD-ES and SK-ES-1 was detected by Western blot, n=3; H, I) The expression of FAM98A in cells with different treatments was detected by qRT-PCR, n=3; Data are presented as the mean±standard deviation. Student's t-test was used for panels A, D, F and I, one-way ANOVA was used for panels B, C, G and H, followed by Tukey's multiple comparisons test. $^{**}p < 0.01$.

Figure 7. miR-107 inhibition partially reverses the suppressive effect of METTL14 knockdown on ES progression. A673 cells were transfected with miR-107 inhibitor (miR-inhi) using inhi-NC as control, followed by combined treatment with sh-METTL14. A) The transfection efficiency was detected by qRT-PCR; B) The expression of miR-107 and FAM98A was detected by qRT-PCR; C) The expression of FAM98A and PCNA was detected by Western blot; D) Cell viability was determined by CCK-8 assay; E) Cell proliferation was evaluated by colony formation assay; Subsequently, cells were co-cultured with macrophages. F) The proportions of $CD86^{+}CD68^{+}$ and $CD206^{+}CD68^{+}$ cells were detected by flow cytometry; G) Transwell lower-chamber macrophage supernatants were harvested and centrifuged; the levels of TNF-α, IL-12, IL-10, and TGF-β in the supernatant were measured by ELISA; H) The expression of iNOS and Arg-1 was detected by

Accepted manuscript

Western blot; n=3. Data are presented as the mean±standard deviation. Student's t-test was used for panel A, one-way ANOVA was used for panels B, E and G, and two-way ANOVA was used for panels C, D, F and H, with Tukey's multiple comparisons test as the post hoc test. *p < 0.05, **p < 0.01

Figure 8. FAM98A overexpression partially reverses the inhibitory effect of METTL14 knockdown on ES progression. A673 cells were transfected with FAM98A overexpression vector (oe-FAM98A) using empty vector (oe-NC) as control, followed by combined treatment with sh-METTL14. A) The transfection efficiency was detected by qRT-PCR; B) The expression of FAM98A was detected by qRT-PCR; C) The expression of FAM98A and PCNA was detected by Western blot; D: Cell viability was determined by CCK-8 assay; E) Cell proliferation was evaluated by colony formation assay; Subsequently, cells were co-cultured with macrophages. F) The proportions of $CD86^{+}CD68^{+}$ and $CD206^{+}CD68^{+}$ cells were detected by flow cytometry; G) Transwell lower-chamber macrophage supernatants were harvested and centrifuged; the levels of TNF-α, IL-12, IL-10, and TGF-β in the supernatant were measured by ELISA; H) The expression of iNOS and Arg-1 was detected by Western blot; n=3. Data are presented as the mean±standard deviation. Student's t-test was used for panel A, one-way ANOVA was used for panels B, E and G, and two-way ANOVA was used for panels C, D, F and H, with Tukey's multiple comparisons test as the post hoc test. *p < 0.05, **p 0.01

Accepted manuscript

679 **Table 1.** PCR primer sequences.

Name	Sequence (5'-3')
METTL14	F: AGTGCCGACAGCATTGGTG
	R: GGAGCAGAGGTATCATAGGAAGC
FOXP4-AS1	F: TGTGTGTCCATCTTCCAGAGC
	R: TGCTAATGTGTAGGGCTGTGG
miR-107	F: GCCGAGCTCTCTGCTTTCAGC
	R: CTCAACTGGTGTCGTGGA
FAM98A	F: GTGCTTGGCTGGTGTCTGAAT
	R: CACTCGGACTGTTAGTTGCTT
U6	F: TCGCTTCGGCAGCACATATACT
	R: AGGTGGCTTTGGTGGAAGAG
GAPDH	F: GGTCCCAGCTTAGGTTCATCA
	R: AATCCGTTCACACCGACCTT

680

Accepted manuscript

Fig. 1 Download full resolution image

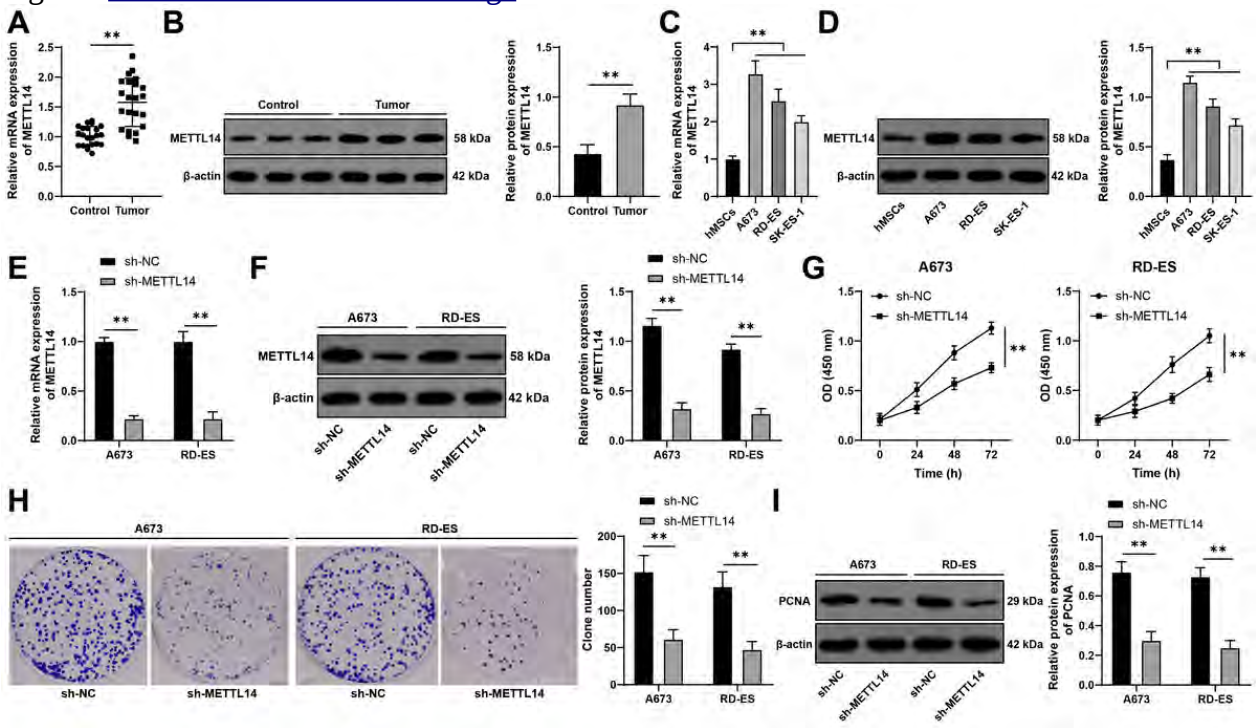

Fig. 2 [Download full resolution image]

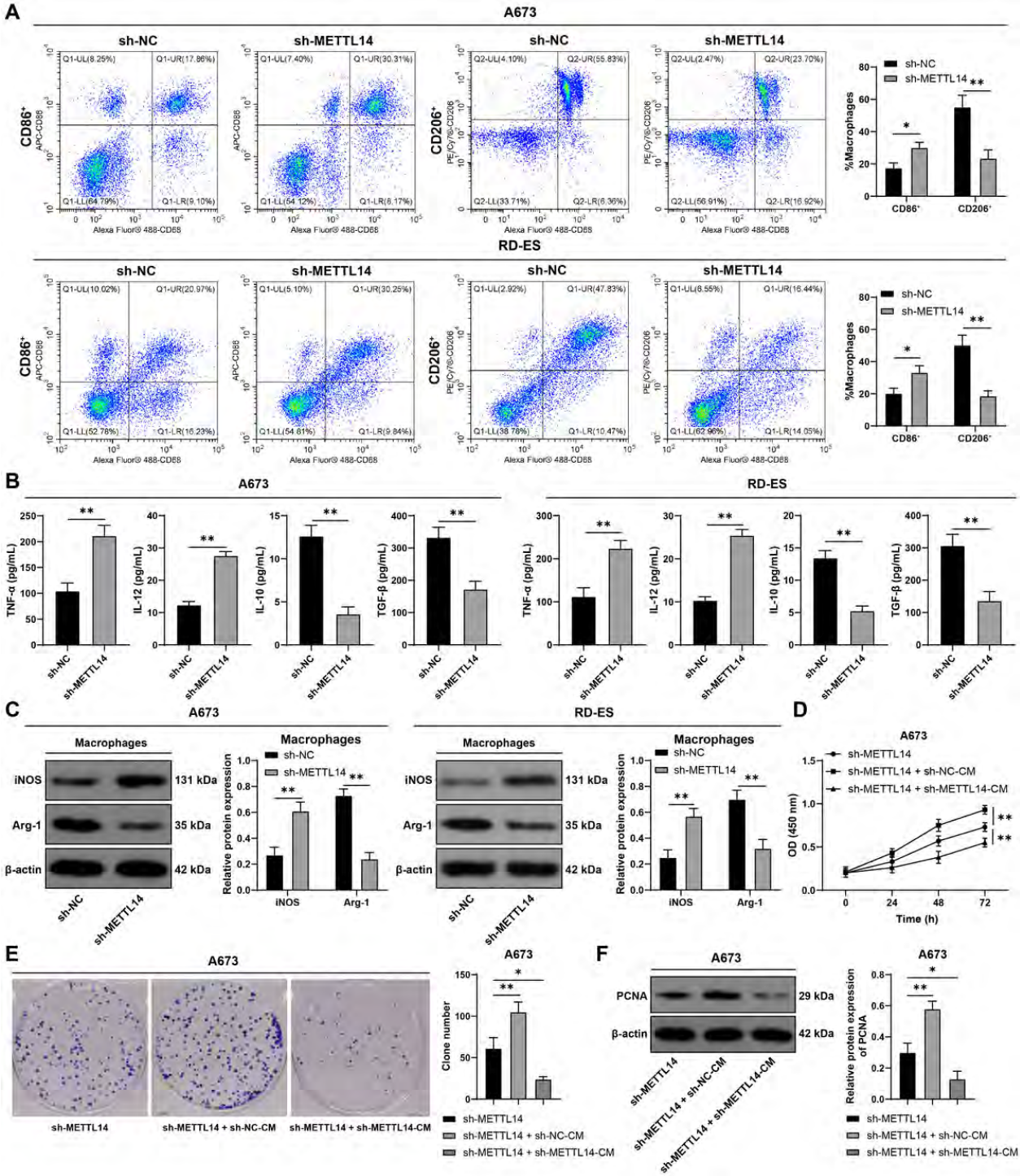

Fig. 3 Download full resolution image

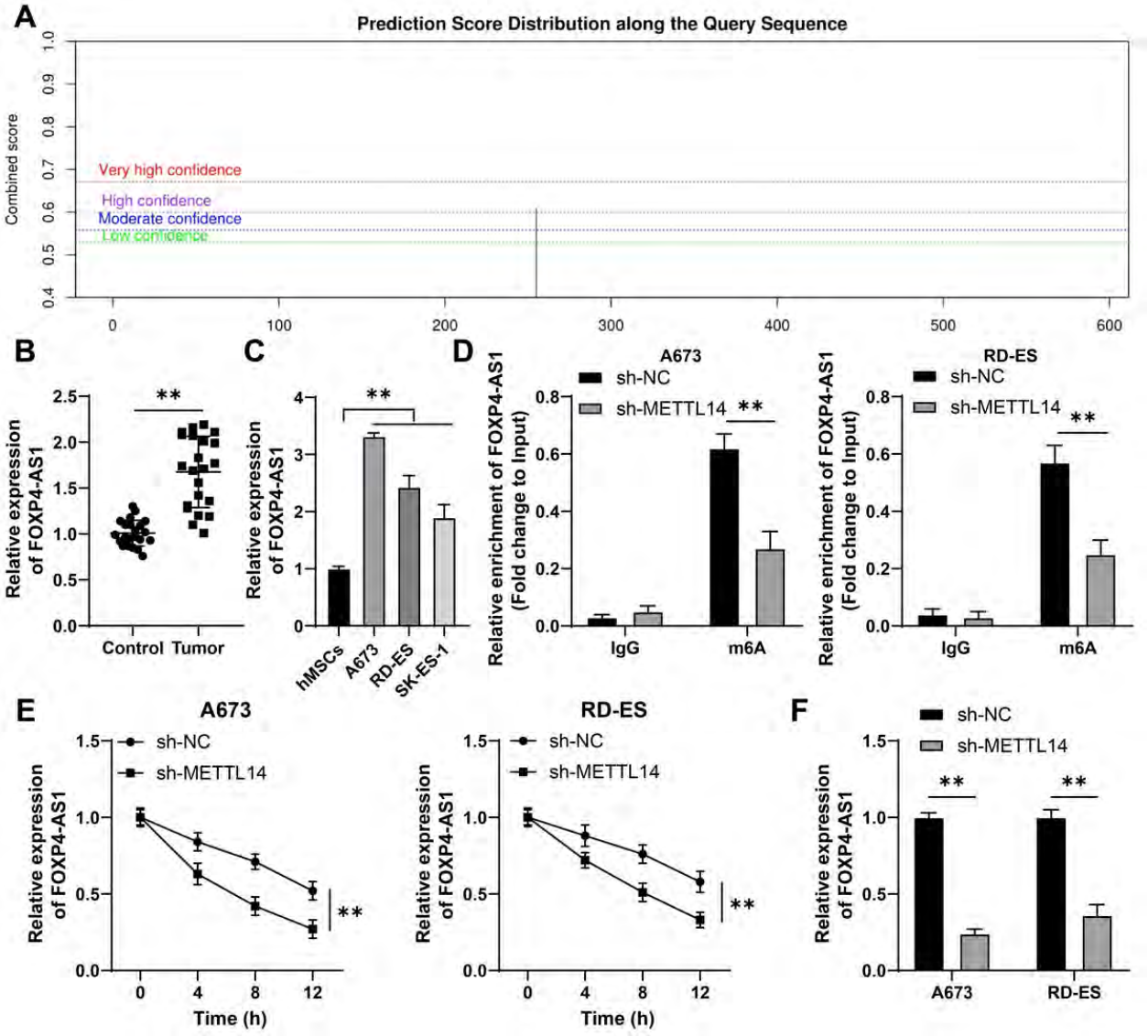

Fig. 4 [Download full resolution image]

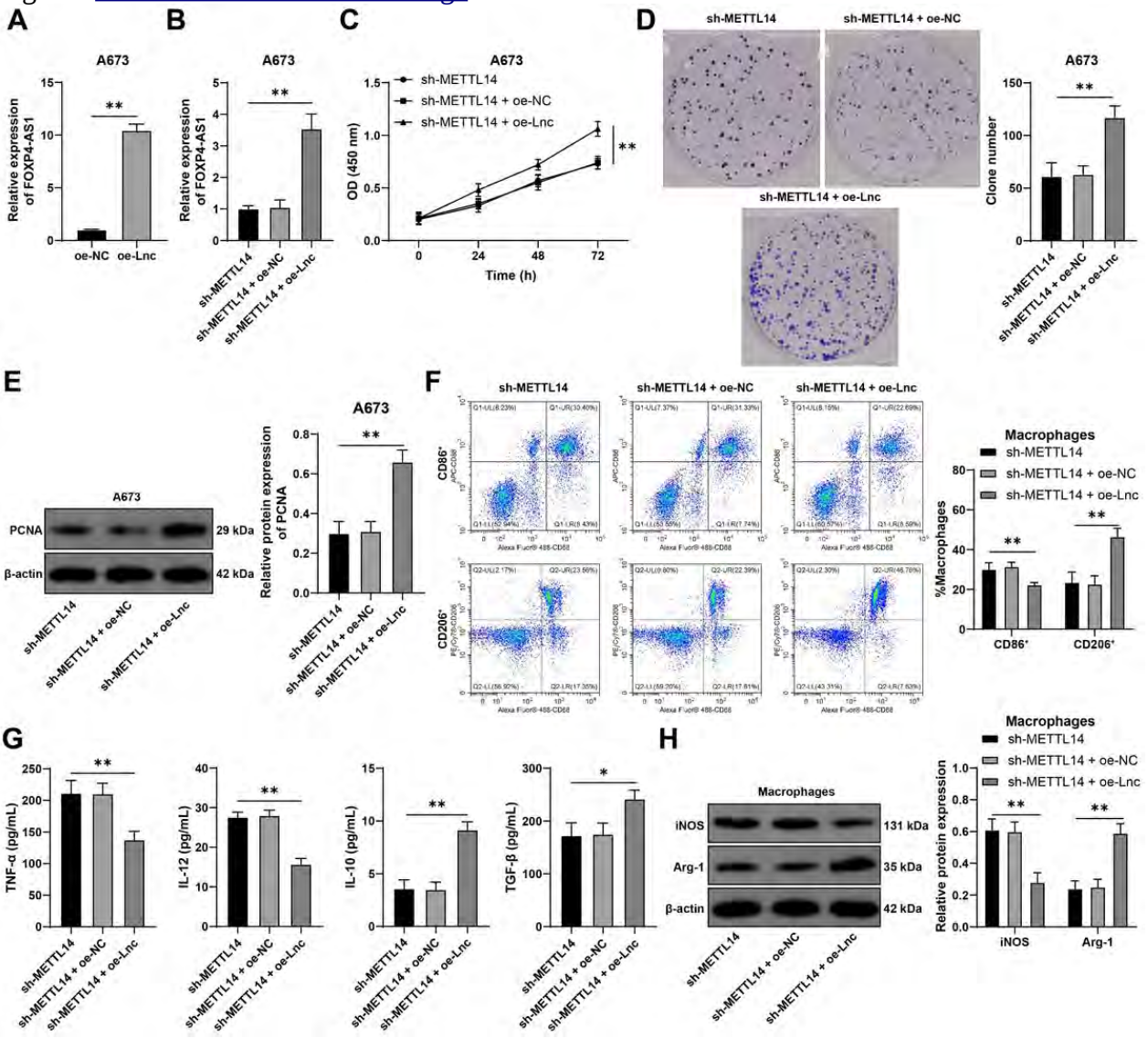

Fig. 5 [Download full resolution image]

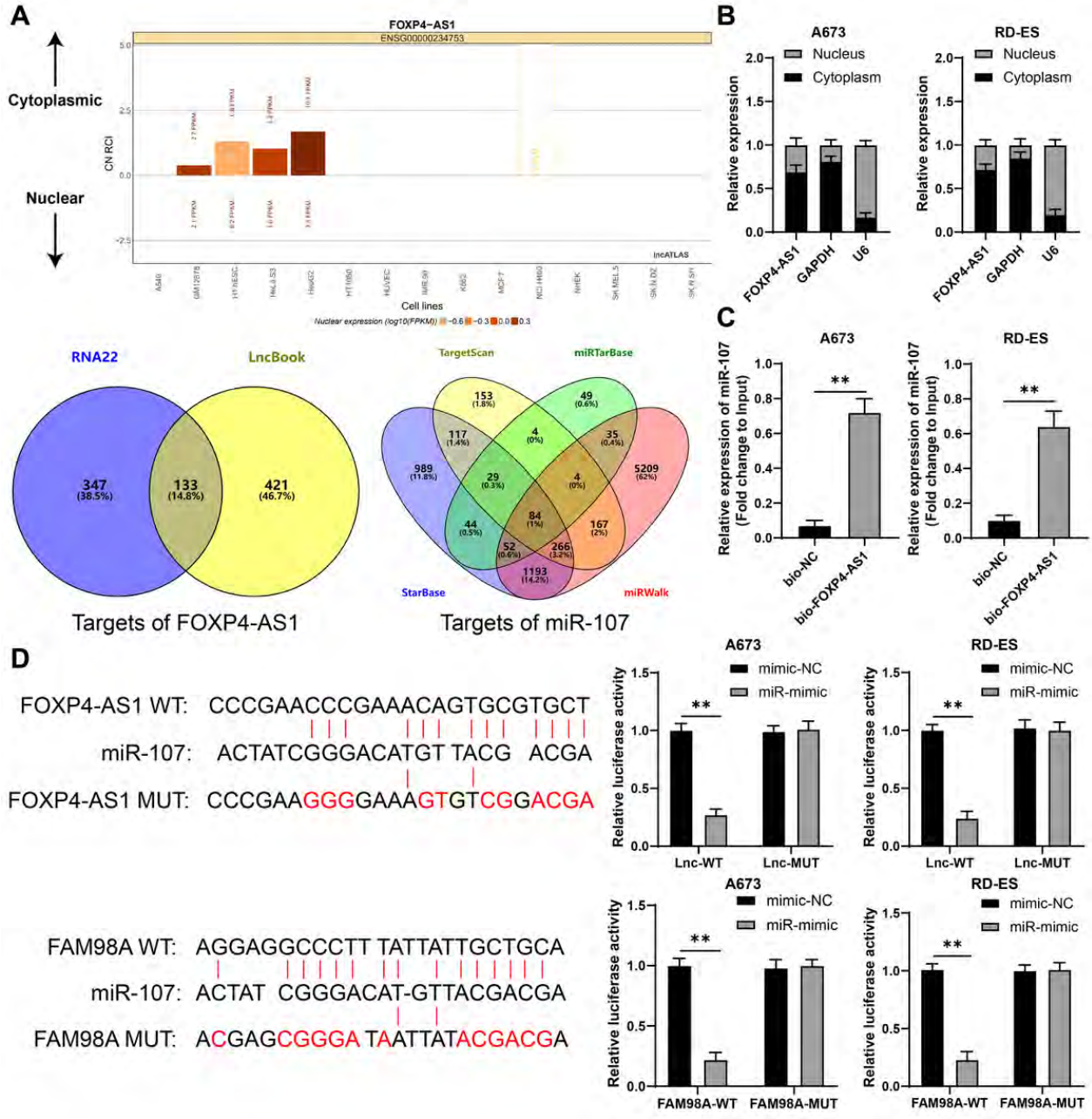

Fig. 6 [Download full resolution image]

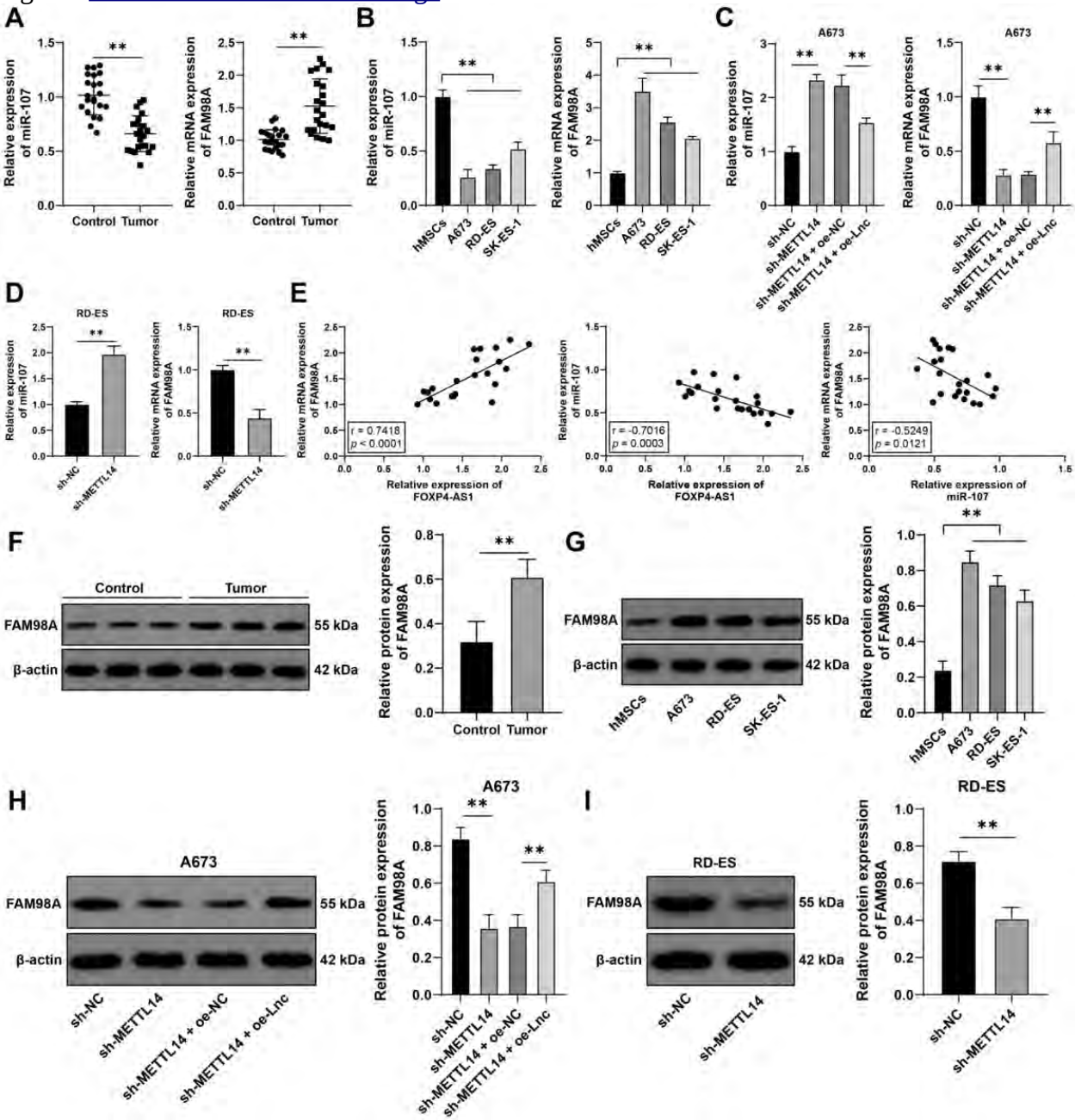

Fig. 7 [Download full resolution image]

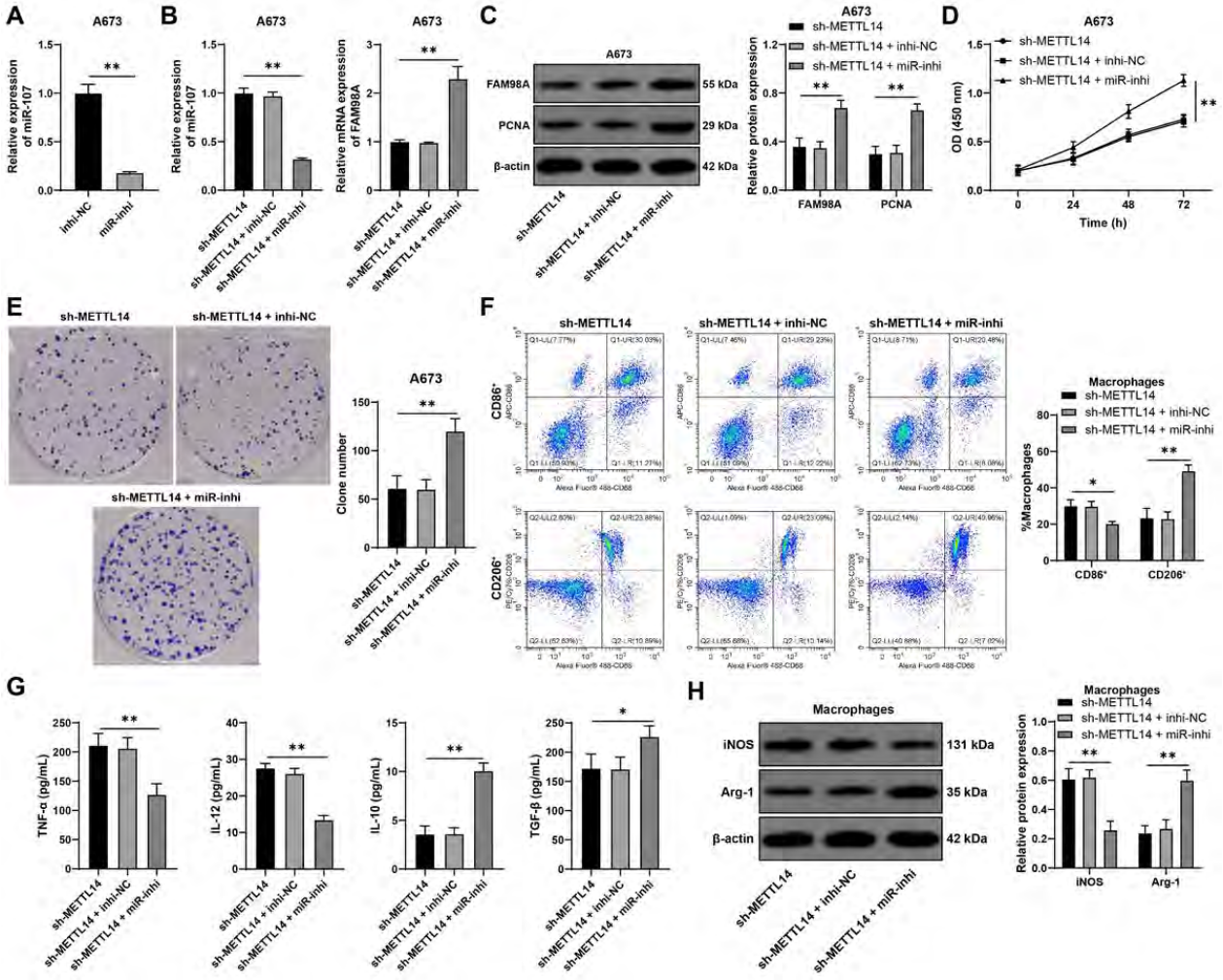

Fig. 8 [Download full resolution image]

